Pergamon

Int. J. Heat Mass Transfer. Vol. 39, No. 9, pp. 1839–1846, 1996

0017-9310/96 $15.00 + 0.00

0017-9310(95)00275-8

Advanced micro-fin tubes for condensation

L. M. CHAMRA and R. L. WEBB†
Department of Mechanical Engineering, Penn State University, University Park, PA 16802, U.S.A.

and

M. R. RANDLETT
Olin Brass Corp., Cuba, MO, U.S.A.

(*Received* 27 *December* 1994 *and in final form* 21 *July* 1995)

Abstract—R-22 condensation data are presented for new micro-fin geometries applied to the inner surface of 15.88 mm outside diameter tubes. The purpose of the work was to develop internal geometries having higher condensation coefficients than existing single-groove micro-fin designs. The new geometries include both single-helix and cross-grooved surfaces. The single-groove geometries have 74–80 internal fins, 0.35 mm fin height, and 30° fin included angle. The cross-groove geometries are formed by applying a second set of grooves at the same helix angle, but opposite angular direction as the first set. Data are provided for varying second groove depths. Data are reported for condensation at 24.0°C in a 2.44 m long test section for 45–181 kg h^{-1} mass flow rate. The data show that the heat transfer coefficient increases with the helix angle, up to the maximum 27° tested. The cross grooved tubes provided higher condensation coefficients than the single-helix geometries. The performance of the new geometries are compared to a single-helix geometry (MX^{TM}-15) similar to existing micro-fin tubes. The best cross-grooved tube provided 27% higher condensation coefficient than the single-helix tube. The pressure drop is 6% higher than in the single helix tube.

INTRODUCTION

This is the second paper in a two paper series reporting the results of work to develop new micro-fin tube geometries for evaporation and condensation. The first paper by Chamra *et al.* [1] reports the evaporation results. This paper addresses the condensation part of the program. The micro-fin tube has found major success in residential air conditioners because of its substantial heat transfer enhancement compared to the pressure drop. This tube, illustrated in Fig. 1, has small fins of triangular cross section at helix angles between 8 and 30° (measured from the tube center line). Refrigerant is either evaporated or condensed in the tube. The tube was first developed by Fujie *et al.* [2] of Hitachi Cable, Ltd and is described by Tatsumi *et al.* [3]. An improved Hitachi design is described by Shinohara and Tobe [4] and by Shinohara *et al.* [5]. The version described by Shinohara and Tobe [4] is close to that now made by tube manufacturers in Japan, Europe and the U.S.A. The tube is made in diameters of 6.35, 7.94, 9.5, or 14.3 and 15.9 mm.

Numerous papers have been published that report the performance of micro-fin tubes. Among these are Schlager *et al.* [6] who reported R-22 evaporation and condensation coefficients and pressure drop for three 12.7 mm outside diameter micro-fin tubes having different helix angles (15, 18 and 25°) with R-22. However, their tubes also had different fin heights ($0.15 \leqslant e_i \leqslant 0.3$ mm) and pitches, and they did not define the effect of specific geometry factors on the performance differences. The effect of geometry factors was investigated by Yasuda *et al.* [7] who investigated the condensation coefficients and pressure drop for 9.52 mm o.d. micro-fin tubes with different fin height, number of fins and helix angle. They reported that the condensation heat transfer coefficient increases with groove depth and helix angle. They also reported an optimum number of grooves between 55 and 60 for the 9.52 mm diameter tube.

Chiang [8] tested four micro-fin tubes having different axial and helical grooves using R-22 as the working fluid. He reported that the condensation heat transfer coefficient for an axial grooved tube is higher than for 18° helical grooves for equal tube diameters. However, the tested tubes had different fin height and apex angle (β), which both have significant effects on the condensation heat transfer coefficient.

The key objective of the present work is to develop higher performance micro-groove geometries for condensation. This paper presents data on the geometries developed for both condensation and evaporation. The performance is compared with that of a plain tube. The plain tube was tested in the present test facility. The tube geometries investigated are described by Chamra *et al.* [1].

† Author to whom correspondence should be addressed.

NOMENCLATURE

A	heat transfer surface area, $A_i/L = \pi(D_0 - 2t_w)$ [m]
D_i	tube inside diameter, or diameter to the base of internal fins or roughness [m]
D_0	tube outside diameter [mm]
e	fin height, roughness height, or corrugation depth [mm]
h	heat transfer coefficient [W m^{-2} K^{-1}]
L	tube length
$\dot{m}$	mass flow rate [kg s^{-1}]
p	axial pitch of surface or roughness elements [mm]
t_w	wall thickness
T_{sat}	saturation temperature [°C].

Greek symbols

α	helix angle relative to tube axis [deg]
β	fin included angle [deg]
η	efficiency index, $(h/h_p)/(\Delta p/\Delta p_p)$
Δp	pressure drop [kPa].

Subscripts

i	designates inner surface of tube
o	designates outer surface of tube
p	plain tube
sat	saturation
w	tube wall.

TEST SECTION GEOMETRIES

Table 1 lists the tube geometries and provides a code for reference to each geometry tested (or compared). The MX™ and MCG™ geometries were manufactured by Olin Brass Corp. Each of the MX™ and MCG™ geometries were made with helix angles (α) of 15, 17.5, 20 and 27°. These geometries are described by a code. For example, MX™-20 indicates a micro-fin tube with single helix geometry having a 20° helix angle, and MCG™-27 indicates a micro-fin tube with cross grooves (MCG™) geometry having a 27° helix angle.

The first set of grooves in the MCG™ tubes are identical to those in the MX™ tubes. However, a second set of grooves is applied to form the cross

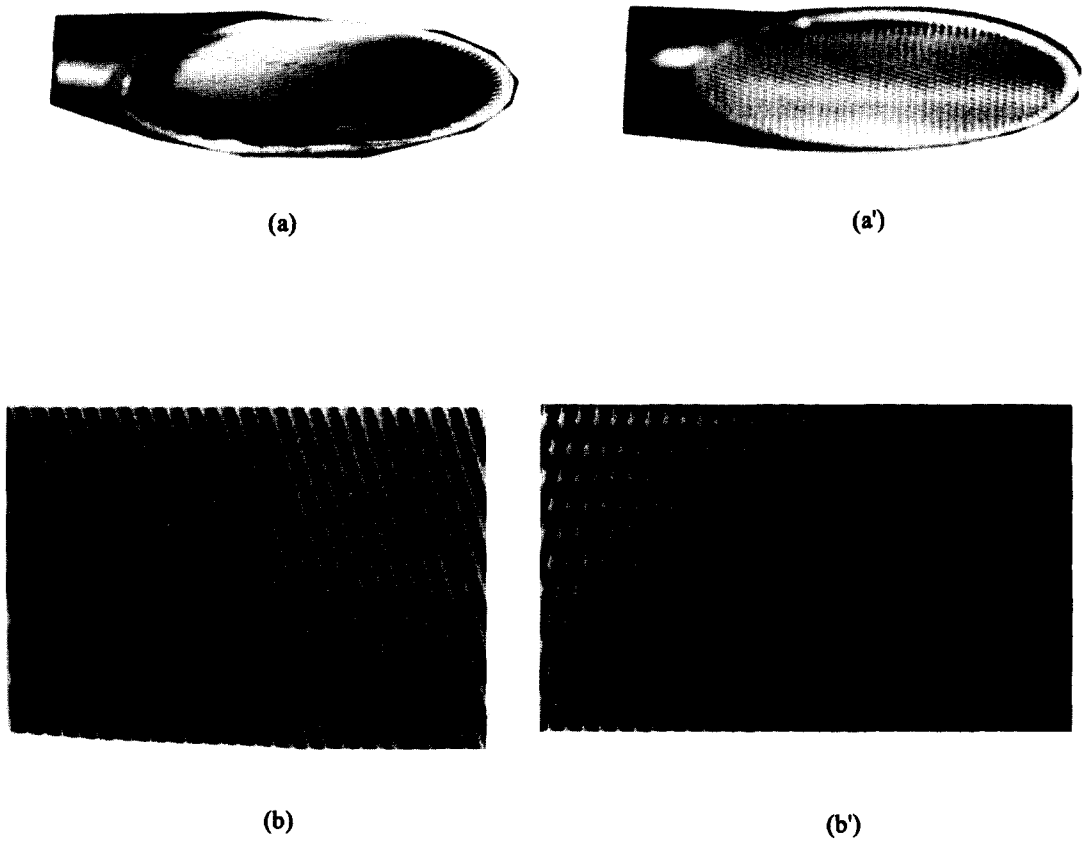

Fig. 1. (a) MX™ micro-fin tube, (b) plain view of MX™ tube, (a′) MCG™ micro-fin tube, (b′) plain view of MCG™ tube.

Table 1. Micro-fin tubes

	MX™ helix	MCG™
Geometry type	Helical	Cross groove
D_0 [mm]	15.88	15.88
D_i [mm]	14.88	14.88
Number of fins	74 at $\alpha = 27°$	74 at $\alpha = 27°$
	78 at $\alpha = 20°$	78 at $\alpha = 20°$
	76 at $\alpha = 17.5°$	76 at $\alpha = 17.5°$
	80 at $\alpha = 15°$	80 at $\alpha = 15°$
Fin height, e [mm] (2nd entry = depth of the second groove set)	0.35	0.35/0.21*
		0.35/0.17
		0.35/0.14*
		0.35/0.07*
Fin pitch, p [mm]	0.58	0.58
Helix angle, α [deg]	15, 17.5, 20, 27	15, 17.5, 20, 27
Fin included angle, β [deg]	30	30
e/D_i	0.024	0.024
p/e	1.66	1.66

* These tubes made with 17.5° helix angle except for 0.35/0.07 which is also made with 27° helix.

groove geometry. The second set of grooves is applied at the same helix angle, but opposite angular direction as the first set. The single helix (MX™) and cross-grooved (MCG™) tubes are shown in Fig. 1. As shown in Table 1, one series of the MCG™ tubes (15, 17.5, 20 and 27) were made with a groove depth 50% that of the first groove (0.17 mm). A second set of MCG™ tubes was also made using 17.5° helix angle, in which the depth of the second set of grooves were made at 20%, 40%, 50%, 60% and 80% depth of the first groove set. Using the coding scheme, a tube having 17.5° helix angle with the second groove set having 50% the depth of the first set is described as MCG™-17.5 @ 50%. A 27° cross-grooved tube was also made with 80% second groove depth (MCG™-27 @ 80%).

TEST APPARATUS

Figure 2 shows a schematic drawing of the apparatus used for in-tube vaporization and condensation. A detailed schematic of the test section is shown in Fig. 3. The apparatus is described in detail by Chamra *et al.* [1] and the description will not be repeated here. For operation in the condensation mode, the R-22 is vaporized in the upstream electric heater. The R-22 in the test section is condensed against cooling water, which flows in the annulus. The R-22 vapor leaving the test section is condensed against R-22 in the heat rejection loop. The sub-cooled condensate is then pumped by a gear pump to the electric heater. The vapor quality entering the test section is calculated using the sub-cooled conditions entering the electric heater and the electric heat input to the boiler.

TEST PROCEDURE AND DATA REDUCTION

The R-22 condensation data were taken at 24°C saturation temperature in the 2.4 m (8 ft) long test section. All data were taken for 80% entering and 20% leaving vapor quality. Sequential points were taken for increasing mass flow rates ($\dot{m}$). The data are plotted as "h vs $\dot{m}$." This is a common method of taking and presenting the data where investigators are to take data for fixed inlet and fixed exit vapor quality in the test section. Use of this method allows comparison of the present test results with published data.

The data reduction procedure described by Chamra *et al.* [9] is also applicable to the condensation data. The condensation coefficients are based on the nominal internal surface area $A_i/L = \pi(D_0 - 2t_w)$, where D_0 is the tube outside diameter, and t_w is the wall thickness at the base of the fins (0.50 mm). This definition facilitates direct comparison of different internal geometries having the same outside diameter and wall thickness. The uncertainties of the measured and calculated parameters are estimated by following the procedures described by Moffat [10]. The error analysis is done for an average mass flow rate and an average heat flux. The experimental uncertainties associated with the sensors and calculated parameters are listed in Table 2.

R-22 CONDENSATION DATA

The apparatus was qualified by testing a plain tube for condensation of R-22. Figure 4 shows the plain tube test results plotted as h vs $\dot{m}$. The data are for 80% entering and 20% leaving vapor quality. Also shown on Fig. 4 is the prediction of Shah [11] at the same saturation temperature, and 70% vapor quality. Figure 4 shows that the present data agree very well with the Shah correlation.

Single-helix geometries (MX™-series)

Figure 5 shows the heat transfer [Fig. 5(a)] and pressure drop [Fig. 5(b)] results for the single-helix MX™-series tubes and for the plain tube. The results of Fig. 5 are summarized in numerical format in Table 3. The Table 3 values are based on smooth curve fits of the Fig. 4 data. This table shows the heat transfer enhancement ratio (h/h_p), the pressure drop ratio ($\Delta p/\Delta p_p$), and the "efficiency index" [$\eta = (h/h_p)/(\Delta p/\Delta p_p)$], where subscript "p" refers to the plain tube. These tabular comparisons are made at 45, 91 and 159 kg h^{-1} mass flow rate.

The only difference among the MX™ tubes shown on Fig. 5 is the helix angle which controls the number of fins. Figure 5 shows that the condensation coefficient (and the pressure drop) increases as the helix angle increases. Figure 6 shows a plot of condensation coefficient and the pressure drop vs helix angle for 136 kg h^{-1} mass flow rate. At 91 kg h^{-1}, Table 3 shows that the heat transfer enhancement ratio (h/h_p) increases from 2.87 to 3.60 as the helix angle is increased from 15 to 27°. The refrigerant pressure drop ratio ($\Delta p/\Delta p_p$) increases from 1.58 to 2.46. Note that ($\Delta p/\Delta p_p$) does not monotonically increase with increasing flow rate. Rather, Table 3

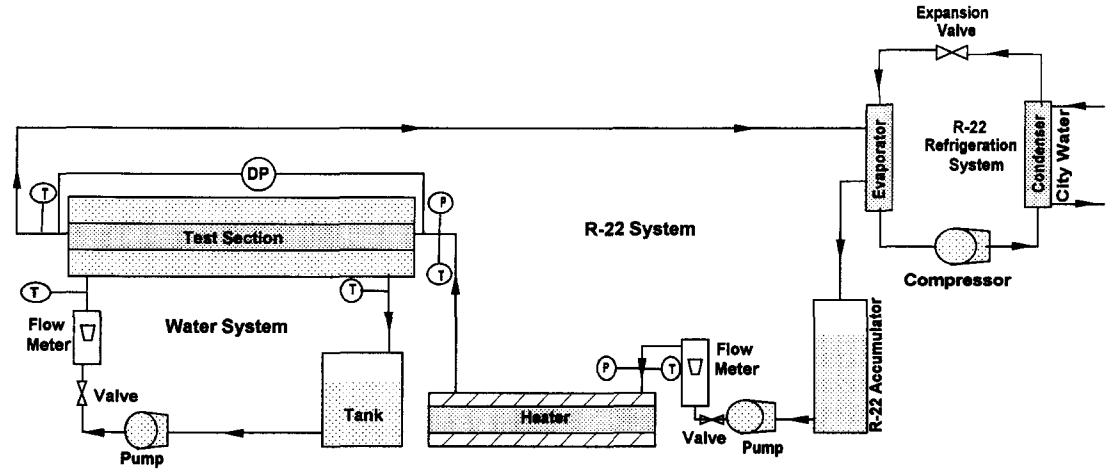

Fig. 2. Schematic drawing of the test facility.

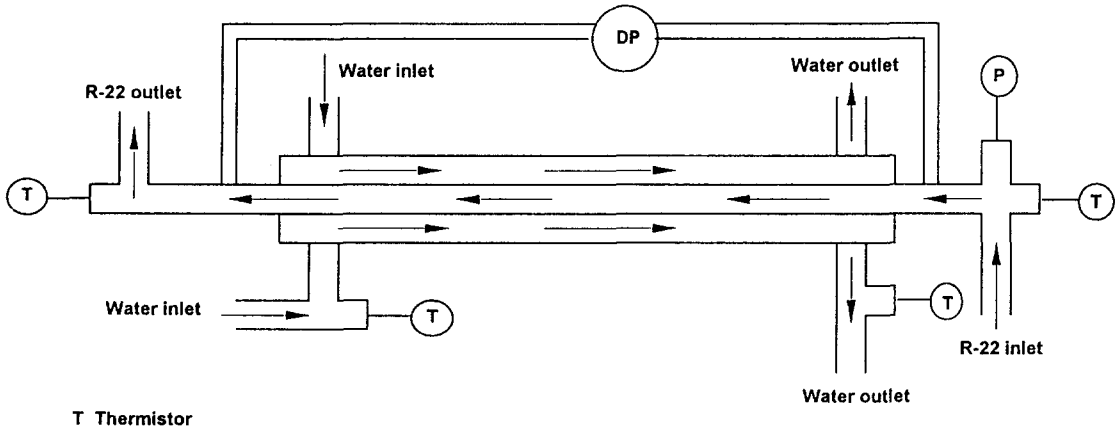

Fig. 3. Detailed schematic of the test section.

Table 2. Experimental uncertainties

Sensors	
Temperature	±0.1 °C
Water flow rate	±1.0 %
Refrigerant flow rate	±1.0 %
Pressure drop	±0.25 kPa
Parameters	
Mass velocity, G [kg m^{-2} s^{-1}]	±2.0 %
Vapor quality, x	±4.1 %
Heat flux, q'' [W m^{-2}]	±5.4 %
Heat transfer coefficient, h [W m^{-2} k^{-1}]	±7.4 %

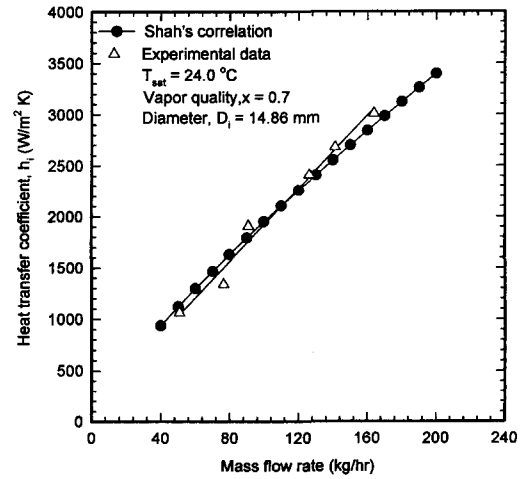

Fig. 4. R-22 condensation heat transfer data for plain tube.

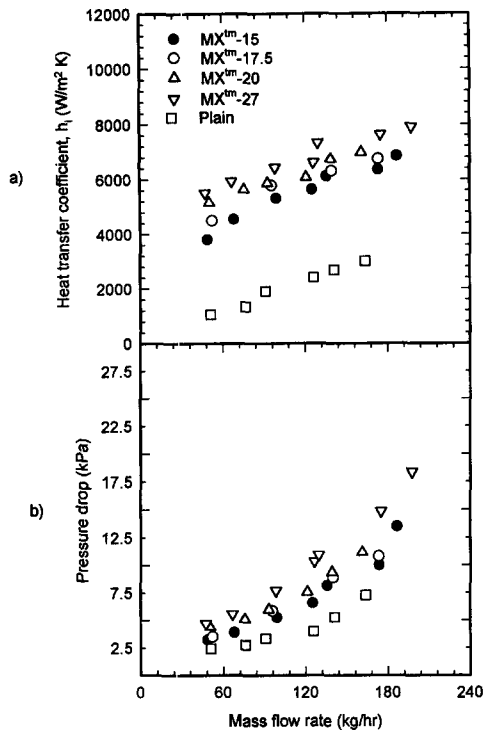

Fig. 5. R-22 condensation data for four MX™ tubes listed in Table 2 (15, 17.5, 20 and 27° helix angles): (a) condensation coefficient; (b) pressure drop.

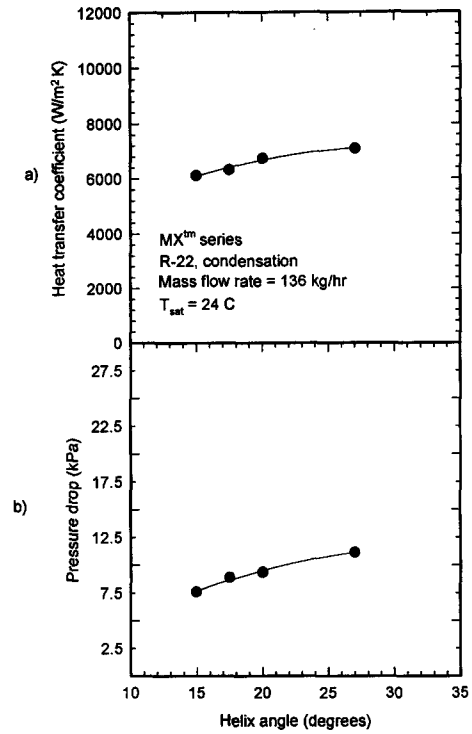

Fig. 6. Variation of R-22 condensation heat transfer coefficient in MX™ tubes with helix angle.

shows that $(\Delta p/\Delta p_p)$ is higher at 91 kg h^{-1} than at 159 kg h^{-1}.

Table 3 shows that the enhancement ratio increases as the flow rate is reduced for all helix angles. For example, the enhancement ratio for the MX™-27 tube is 5.90 at 45 kg h^{-1}, as compared to 2.49 at 159 kg h^{-1}. Further examination of Table 3 shows this behavior occurs for all of the geometries tested. This behavior also occurred for evaporation. For fixed helix angle, the pressure drop ratio $(\Delta p/\Delta p_p)$ increases only modestly with increasing flow rate. Hence, the efficiency index $[\eta = (h/h_p)/(\Delta p/\Delta p_p)]$ decreases as the flow rate increases.

Cross-grooved tubes (MCG™-series)

In these tubes, a second set of grooves was cut, at the opposite angle to the first set. The depth of the second set of grooves is an additional geometric parameter. Two different geometry variants were investigated for the MCG™ geometry. In the first series, the depth of the second set of grooves was held at 50%, and the helix angle was varied. In the second series, the helix angle was held at 17.5° and the depth of the second groove set was varied from 40% to 80%. The term 80% means the second set of grooves is 80% that of the first set.

Figure 7(a) shows the data for the MCG™ tubes with 50% second groove depth. The data are also listed in Table 3. The condensing coefficient of the MCG™ geometry increases with helix angle, as for the MX™ geometry. Referring to Table 3, one sees that, for the same helix angle, the MCG™ @50% geometries provide greater enhancement than the corresponding MX™ geometry. At 91 kg h^{-1}, the con-

Table 3. Heat transfer and pressure drop ratios (R-22 condensation in 2.4 m long test section)

	$\dot{m}$ = 45 kg h^{-1}			$\dot{m}$ = 91 kg h^{-1}			$\dot{m}$ = 159 kg h^{-1}		
	h/h_p	$\Delta p/\Delta p_p$	η	h/h_p	$\Delta p/\Delta p_p$	η	h/h_p	$\Delta p/\Delta p_p$	η
MX™-15	4.00	1.26	3.17	2.87	1.58	1.82	2.14	1.44	1.49
MX™-17.5	4.56	1.20	3.80	3.17	1.95	1.62	2.23	1.49	1.50
MX™-20	5.40	1.64	3.29	3.28	1.95	1.68	2.34	1.64	1.43
MX™-27	5.90	1.73	3.41	3.60	2.46	1.46	2.49	2.01	1.24
MCG™-15 @ 50%	4.50	1.41	3.19	3.10	1.93	1.60	2.28	1.63	1.40
MCG™-17.5 @ 50%	4.98	1.42	3.50	3.48	2.07	1.68	2.40	1.74	1.38
MCG™-20 @ 50%	5.88	1.70	3.45	3.66	2.14	1.70	2.59	1.91	1.36
MCG™-27 @ 50%	6.17	1.95	3.16	3.93	2.76	1.42	2.72	2.13	1.27
MCG™-27 @ 80%	6.78	2.12	3.20	4.32	2.80	1.54	2.98	2.40	1.24

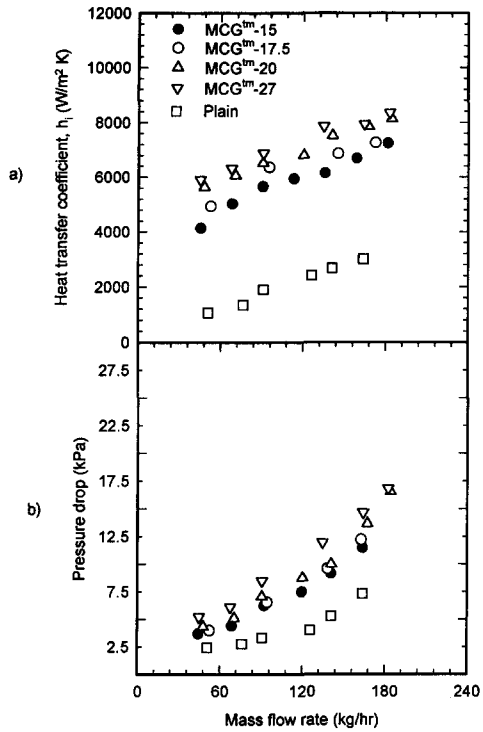

Fig. 7. R-22 condensation data for four MCG™ @50% tubes listed in Table 2 (15, 17.5, 20 and 27° helix angles): (a) condensation coefficient; (b) pressure drop.

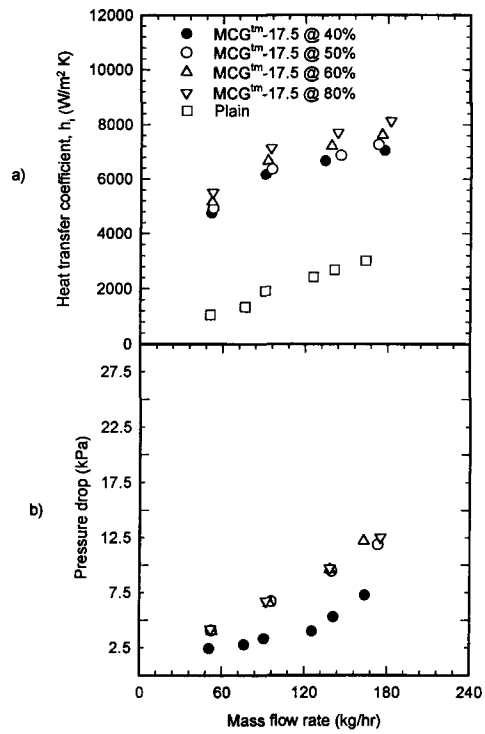

Fig. 8. R-22 condensation data for four MCG™ 17.5 tubes listed in Table 2 with different second groove depth (40%, 50%, 60% and 80%): (a) condensation coefficient; (b) pressure drop.

densing coefficient of the MCG™ tube is nominally 10% higher than that of the MX™ geometry for all helix angles. Figure 7(b) shows the pressure drop of the MCG™ @50% geometries. Table 3 shows that the pressure drop increase, relative to the MX™ geometry, is nearly proportional to the heat transfer increase. Hence the efficiency index of the MCG™ and MX™ tubes (for the same helix angle) is approximately equal.

Figure 8 shows the performance data for the 17.5° helix angle MCG™ geometry with varying second groove depth. The second groove depths shown on Fig. 8 are 40%, 50%, 60% and 80%. Figure 8(a) shows that the condensation coefficient increases as the depth of the second groove set increases. These data are also shown in Table 4, along with data for the MX™-17.5 geometry. The addition of a second groove set provides higher performance than the single helix MX™ geometry. As shown in Table 4, the MCG™ geometry with 80% groove depth provides 24% higher condensation coefficient than the single helix MX™ geometry. This enhancement level is approximately constant at all flow rates. In addition to its higher heat transfer performance, the MCG™ geometry also shows a higher efficiency index than the MX™ geometry. Thus at 91 kg h^{-1}, the 24% condensation coefficient increase is accompanied by only 9% pressure drop increase. The pressure drop data for the MCG™-17.5 @50% geometries are shown in Fig. 8(b). Table 4 shows that the efficiency index of the MCG™ geometry increases as the second groove depth increases.

The data show that the condensation coefficient increases with increasing helix angle and increasing second groove depth. Hence, one final MCG™ geometry was made and tested. This MCG™ geometry was made with 27° helix angle and 80% second groove depth (tube MCG™-27 @80%). Table 3 lists the performance of the MCG™-27 @80% geometry. At 91 kg h^{-1}, Table 3 shows that this tube provides 36% higher condensation coefficient than the single helix MX™-17.5 geometry. Or, at the same helix angle (27°), the condensation coefficient of the MCG™-27 @80% geometry is 20% higher than the MXTM-27 tube. However, the efficiency index of the MCG™-27 @80% geometry is lower than that of the MX™-17.5 and the MX™-27 single helix geometries.

The high performance of the cross-grooved tubes may be because of the increased number of condensate drainage points, and the increased surface area provided by the second set of grooves is beneficial to condensation. It is speculated that surface tension force is an important factor in draining condensate from the tips of the fins. This may be expected at moderate to high vapor qualities, where the microfins are not flooded by condensate.

Summary comparison

Figure 9 provides a summary comparison of the highest performing tubes for each geometry series.

Table 4. Heat transfer and pressure drop ratios for different second groove depth (R-22 condensation in 2.4 m long test section)

	$\dot{m} = 45$ kg h^{-1}			$\dot{m} = 91$ kg h^{-1}			$\dot{m} = 159$ kg h^{-1}		
	h/h_p	$\Delta p/\Delta p_p$	η	h/h_p	$\Delta p/\Delta p_p$	η	h/h_p	$\Delta p/\Delta p_p$	η
MX™-17.5	4.56	1.20	3.80	3.17	1.95	1.62	2.23	1.49	1.50
MCG™-17.5 @ 40%	4.84	1.42	3.41	3.43	2.14	1.60	2.35	1.61	1.46
MCG™-17.5 @ 50%	4.98	1.42	3.50	3.48	2.07	1.68	2.40	1.74	1.38
MCG™-17.5 @ 60%	5.24	1.47	3.56	3.69	2.21	1.67	2.54	1.66	1.53
MCG™-17.5 @ 80%	5.59	1.45	3.86	3.91	2.12	1.84	2.70	1.59	1.70

The highest performance for each geometry occurs at 27° helix angle. Figure 9(a) clearly shows the superiority of the MCG™ @80% geometry, relative to the single-grooved MX™ geometries. Figure 9(b) shows that the pressure drop increase of the MCG™ @80% geometry is small compared to the heat transfer increase shown on Fig. 9(a).

EVAPORATION VS CONDENSATION

It is of value to compare the enhancement levels obtained for evaporation and for condensation with the same tube geometries. This comparison is facilitated using the data of Chamra *et al.* [1], who measured R-22 evaporation at 2.22°C in the same geometries and at the same flow rates. With certain exceptions, the order of the h/h_p data vs geometry were the same for condensation and evaporation. A geometry that provides high condensation enhancement also provides high evaporation enhancement. However, the following exceptions were observed:

(1) For evaporation, the enhancement decreased for helix angles greater than 20°. This is true for both the MX™ and MCG™ geometries.

(2) For evaporation, the enhancement in the MCG™ geometry decreased when the depth of the second groove set exceeded 60%. It is possible that the fin tips for the 80% second groove depth de-wetted. Dewetting is not a concern for condensation, because the condensate wets the surface.

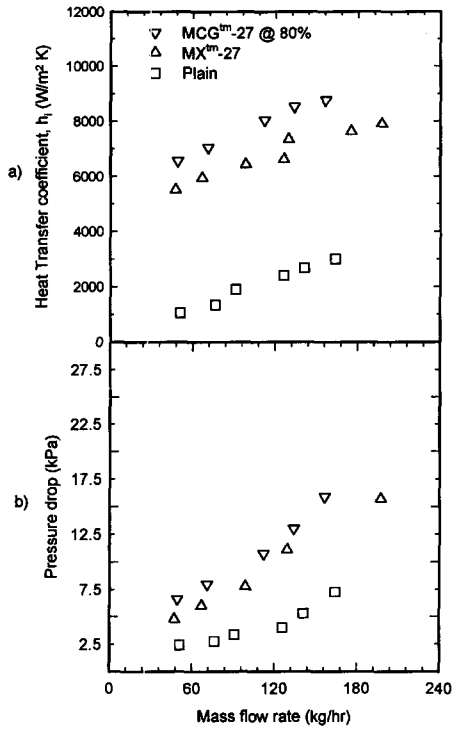

Fig. 9. Comparison of R-22 condensation coefficients in best performing tubes compared with plain tube: (a) condensation coefficient; (b) pressure drop.

Chamra and Webb [11] tested the MCG™-15 @50% geometry in evaporation and condensation at the same saturation temperature (24.4°C). These tests showed that the condensation and the evaporation coefficients were nominally equal for vapor qualities greater than 50%. At lower vapor qualities, the evaporation coefficient tended to be a little greater than the condensation coefficient. It was speculated that nucleate boiling may be responsible for this difference. If the fins are wetted, and nucleate boiling contributions are absent, it appears that the mechanism of evaporation and condensation are the same. Both vaporization and condensation show a small effect of heat flux in the high vapor quality regions.

APPLICATION CONSIDERATIONS

The highest heat transfer coefficients were provided by the single-helix MX™-27 geometry and the cross-grooved MCG™-27 at 80% tube. However, the pressure drop is also an important factor in design consideration. For fixed compressor discharge pressure, refrigerant pressure drop will reduce the driving temperature difference. Typically, a larger pressure drop can be tolerated in a condenser than an evaporator. Refrigerant pressure drop will reduce the saturation temperature in accordance with the equation $\Delta T_{sat} = (dT/dp)\Delta p$. For an R-22 evaporator saturation temperature of 2.2°C, dT/dp is approximately 2.5 times that at 48°C condensing temperature. So, one could accept 2.5 times the pressure drop in a condenser as in an evaporator for the same drop in saturation temperature.

Whether a given tube geometry is useful depends

on whether the designer has freedom of selecting the flow rate/circuit, or whether it is a fixed value. For consideration of an existing design, one should consider the flow rate/circuit is a fixed value. So, one should be able to use a candidate tube geometry if its heat transfer performance is at least as good as the existing tube and the pressure drop is no higher.

CONCLUSIONS

(1) This work has resulted in the identification of new "micro-grooved" tube geometries that provide higher performance for R-22 condensation than certain existing commercial products. The advanced tube geometries also have higher pressure drop. However, the pressure drop increase is less than the heat transfer coefficient increase.

(2) For both single and cross-grooved geometries, the heat transfer and pressure drop increases as the groove helix angle increases, up to the maximum value of 27° tested.

(3) The MCG™ (cross-grooved) tubes exhibit higher heat transfer performance than the MX™ (single groove) tube for all second groove depths.

(4) For the MCG™ tubes, the condensation heat transfer coefficient increases as the depth of the second groove increases. The depth of the second grooves has little effect on the pressure drop.

(5) The highest heat transfer performance tube has cross-grooves 80% of the depth of the first grooves, and 27° helix angle. This tube provides 51% higher condensation coefficient than the 15°, single-helix MX™-15 tube. However, the pressure drop is about 77% higher pressure drop at 91 kg h^{-1}.

Acknowledgements—The authors would like to express their thanks to Olin Brass for supporting this project and providing the tubes. We would also like to acknowledge that Wolverine Tube, Inc. donated the apparatus on which the data were taken.

REFERENCES

1. L. M. Chamra, R. L. Webb and M. R. Randlett, Advanced micro-fin tubes for evaporation, *Int. J. Heat Mass Transfer* **39,** 1827–1838 (1996).
2. K. Fujie, N. Itoh, T. Innami, H. Kimura, N. Nakayama and T. Yanugidi, Heat transfer pipe. U.S. Patent 4 044 797, assigned to Hitachi Ltd (1977).
3. A. Tatsumi, K. Oizumi, M. Hayashi and M. Ito, Application of inner groove tubes to air conditioners, *Hitachi Rev.* **32**(1), 55–60 (1982).
4. Y. Shinohara and M. Tobe, Development of an improved thermofin tube, *Hitachi Cable Rev.* **4,** 47–50 (1985).
5. Y. Shinohara, K. Oizumi, Y. Itoh and M. Hori, Heat transfer tubes with grooved inner surface. U.S. Patent 4 658 892, assigned to Hitachi Cable Ltd (1987).
6. L. M. Schlager, M. B. Pate and A. E. Bergles, Evaporation and condensation heat transfer and pressure drop in horizontal, 12.7-mm micro-fin tubes with refrigerant 22, *J. Heat Transfer* **112,** 1041–1047 (1990).
7. K. Yasuda, K. Ohizumi, M. Hori and O. Kawamata, Development of condensing thermofin-HEX-C tube, *Hitachi Cable Rev.* **9,** 27–30 (1990).
8. R. Chiang, Heat transfer and pressure drop during evaporation and condensation of refrigerant-22 in 7.5 mm diameter axial and helical grooved tubes, *A.I.Ch.E. Symp. Ser.* 295, **89,** 205–210 (1993).
9. L. M. Chamra and R. L. Webb, Condensation and evaporation in micro-fin tubes at equal saturation temperatures, *J. Enhanced Heat Transfer* **2**(3), 219–229 (1995).
10. Robert J. Moffat, Describing the uncertainties in experimental results, *Exp. Thermal Fluid Sci.* **1,** 3–17 (1988).
11. M. M. Shah, A general correlation for heat transfer during film condensation in tubes, *Int. J. Heat. Mass Transfer* **22**(4), 547–556 (1979).